J Mater Sci (2007) 42:10288–10295
DOI 10.1007/s10853-006-0576-8

# Synthesis of zirconium diboride–zirconium nitride composite powders by self-propagating high-temperature synthesis

**H. E. Çamurlu · F. Maglia**

Received: 15 February 2006 / Accepted: 14 June 2006 / Published online: 22 September 2007


**Abstract** Formation of zirconium diboride–zirconium nitride composite powders by self propagating high temperature reaction of zirconium, boron and hexagonal boron nitride powders was investigated. Zirconium diboride–zirconium nitride powder mixtures with varying proportions were produced by changing the amount of boron nitride in the reactants. Products were subjected to powder X-ray diffraction analysis; and grain size and morphology was examined by scanning electron microscope. It was seen that the velocity of the wave front, adiabatic temperature of the reaction and grain size of the products decreased by increasing the boron nitride amount in the reactants. It was deduced from the scanning electron microscope examinations and crystal size calculations performed from the broadening of the peaks on the X-ray diffractions patterns that zirconium nitride grains were much finer than zirconium diboride grains.

## Introduction

Zirconium diboride ($ZrB_2$) exhibits excellent properties such as high melting point, high strength and hardness (25.3–28 GPa) [1], high thermal and electrical conductivity, resistance to oxidation and thermal shock [2]. Combination of the high temperature properties of $ZrB_2$ with its outstanding resistance to chemicals like HCl, HF and various molten non-ferrous metals and non-basic slags, makes it an ideal refractory material. Some other applications of $ZrB_2$ are high temperature structural materials, ballistic armors, coating for cutting tools and as an anti-oxidant additive [3]. Zirconium nitride (ZrN) has low friction coefficient and high hardness (15 GPa) [4]. In addition to these properties, due to its high wear and corrosion resistivity and high thermal conductivity, ZrN is used as hard coatings in cutting tool appliances, injection molds and extrusion dies [4]. Some of the production techniques of $ZrB_2$ are the reaction between elemental powders [5, 6], metallothermic reduction of boric oxide and zirconium oxide through self-propagating high-temperature synthesis (SHS), arc melting, vapor deposition, plasma synthesis [2, 3, 7]. ZrN is produced in powder form by nitridation of Zr metal with ammonia or nitrogen gas at 1200 °C [3].

SHS is a technique that utilizes the heat evolving from the exothermic reactions taking place between the reactants, which are mixed and shaped as a loose pellet. The only energy supplied to the system is the heat from the igniter coil to start up the reaction. Once started, the reaction self-propagates, as a combustion front, through the reactive pellet, resulting in a product phase or a mixture of phases. The use of simple equipment, low energy requirements and high purity of the products are some of the advantages that makes SHS technique [2] an appealing method for producing various materials in a wide range of systems such as intermetallics, oxide and non-oxide type ceramics, etc. [7, 8]. The only limitation of this method is that it can only be applied in highly exothermic systems, i.e. $\Delta H$ = –40kcal/mol.

Previous studies investigated the SHS of Zr-based refractory composite materials [5, 6, 9–11]. In the studies of

H. E. Çamurlu (✉)
Department of Mechanical Engineering, Akdeniz University, Dumlupınar Bulvarı, Antalya 07058, Turkey
e-mail: erdemcamurlu@gmail.com

F. Maglia
Department of Physical Chemistry, University of Pavia, V.1e Taramelli, 16, Pavia 27100, Italy

Radev et al., relationship between properties of reagents and products was explored in the Zr–B and Ti–B systems [5, 6]. In another SHS study, the synthesis of ZrC–ZrN mixtures was performed through auto ignition and SHS, by subjecting mechanically activated Zr and C powders to air [9]. It was reported that only a minor amount of ZrN could be formed in the system, most of which was on the upper part of the mixture being in contact with air. At the same time, high concentration of unreacted zirconium remained in the products. This implies the reluctance of gaseous nitrogen at atmospheric pressure in reacting with zirconium.

It was reported that the fracture toughness and flexural strength of $ZrB_2$ based composites could be improved considerably with the addition of a second reinforcing phase [12]. The aim of the present study is to investigate the formation of $ZrB_2$ and ZrN powder mixtures by the SHS technique. The low amount of ZrN in the products obtained in the previous studies due to low reactivity of Zr with the gaseous nitrogen in air (or with pure gaseous nitrogen at 1 atm.) lead us to consider a nitrogen bearing compound to be included in the reactants. Hexagonal boron nitride (BN) could be the best candidate for the purpose of the present study, since it is a source of both boron and nitrogen, and leaves no residual side products. The SHS reaction of Zr, B and BN was studied by altering the proportions of Zr and BN in the reactants in order to obtain $ZrB_2$–ZrN composite powder mixtures with varying ratios of the constituents.

BN has been successfully used in the synthesis of $TiB_2$–TiN composite materials leading to the formation of homogeneous and well dispersed grains of the two components [13]. In two recent studies, reactive hot pressing (RHP) technique has been utilized in order to produce $ZrB_2$–ZrN monolithic composites [14, 15]. RHP involved simultaneous heating and pressing of the Zr–BN reactants at 1650–1900 °C under 20–30 MPa pressure for 1–2 h. This technique aims the production of compacted articles with high densities and requires rather expensive equipment. During this process, the heating rate has to be kept below 10 °C/min in order to avoid a combustion reaction and heating should be applied continuously [14]. The heat of reaction evolves slowly and is dissipated in the surroundings, hence no ignition occurs. However, in SHS very small energy is introduced into the system to initiate the reactions, the products are formed instantaneously and the products are almost always porous when no additional means of compaction is applied and when the melting points of the products are high. Therefore the RHP method is entirely different from the SHS technique in terms of the form and production rate of the products and energy utilization. SHS has been utilized for the synthesis of many similar composite systems such as $ZrB_2$–$Al_2O_3$–Al [7], ZrC–ZrN [9], ZrC–$ZrB_2$ [10], $TiB_2$–TiN [13]. To the best of our knowledge, there is no data in the literature pertaining to the characteristics of SHS processing of the ZrN–$ZrB_2$ composite powders.

Both of the phases constituting the composite powders produced in the present study can withstand very high temperatures and have high hardness. These composite powders, produced by the intimate combination of these phases and having excellent properties, are suitable to be utilized in powder form in various applications such as abrasive media and reinforcements in metal matrix composites. Moreover, powders produced by SHS are often reported to show higher reactivity and enhanced sinterability due to high defect concentrations produced by the very high heating and cooling rates attained in the SHS process [16–18]. Therefore, in addition to their utilization in powder form, $ZrB_2$–ZrN composite powders can also be sintered into shaped products by hot pressing (HP).

## Experimental procedure

The reactants used in this study were Zr powder (95%, Alfa Aesar), B powder (90%, Alfa Aesar), BN powder (99%, Sigma Aldrich). The grain size and morphology of the starting materials were investigated by scanning electron microscopy (SEM). These properties of the starting materials were of interest because of their possible affect on the grain size and morphology of the product phases. SEM images of Zr powder, B powder, and BN powder are presented in Fig. 1(a–c), respectively. It is seen on these micrographs that Zr powder has a grain size below 3 μm and B has an even finer microstructure. BN powder has plate shaped grains with diameters in the range of 1–8 μm and thickness of a few hundred nanometers.

Two batches of reactant powder mixtures were prepared. The first one consisted of Zr and B and the second Zr and BN in the stoichiometric amounts required by Reactions (1) and (2). The two batch mixtures were mixed in various ratios to obtain $ZrB_2$–ZrN composites with different proportions of the constituting phases as shown in Table 1. Thus, the overall reaction taking place during SHS can be shown as Reaction (3). The adiabatic temperatures of all mixtures, calculated by the HSC software [17], are listed in Table 1.

$$Zr + 2B = ZrB_2 \qquad \text{Reaction (1)}$$

$$3Zr + 2BN = ZrB_2 + ZrN \qquad \text{Reaction (2)}$$

$$(1 + 3x/2)Zr + 2B + (x)BN = (1 + x/2)ZrB_2 + (x)ZrN \qquad \text{Reaction (3)}$$

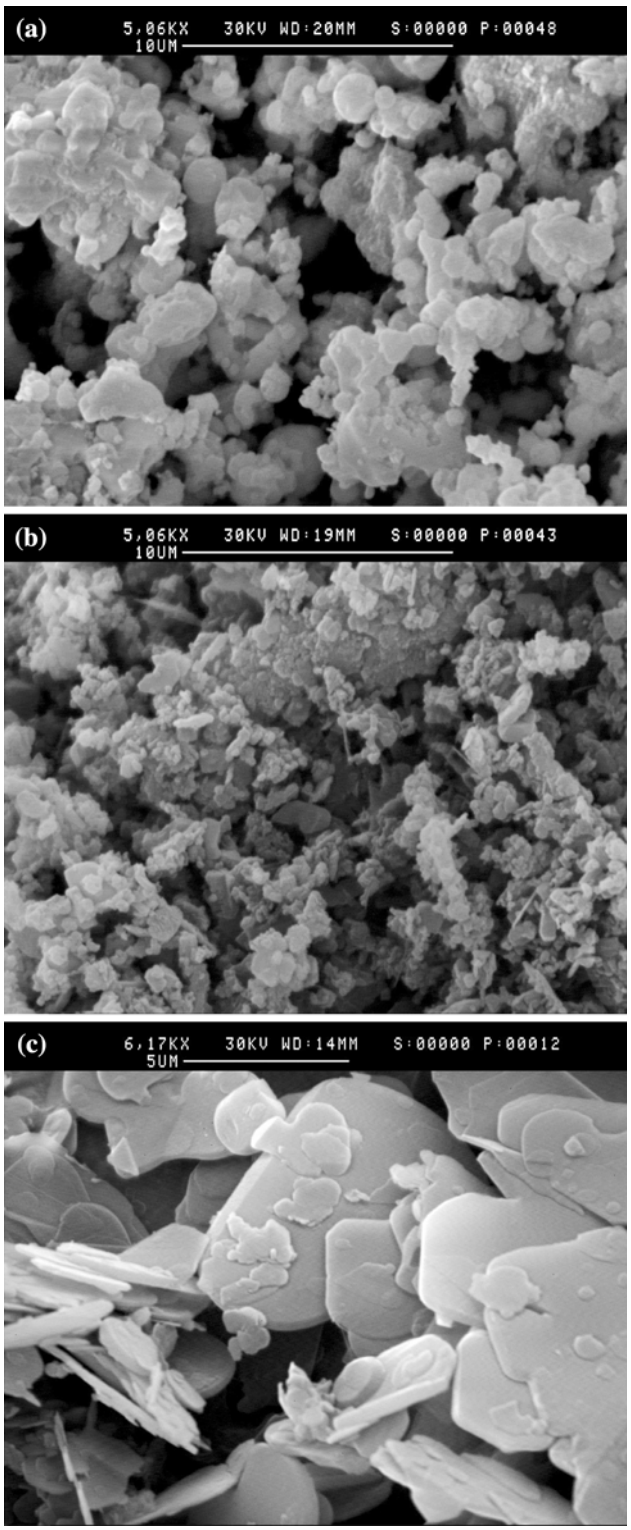


**Fig. 1** SEM micrographs of the starting materials used in the SHS reactions. (**a**) Zr powder (×5060), (**b**) amorphous B powder (×5060), (**c**) BN powder (×6170)

The reactants powders were thoroughly dry mixed then uniaxially cold pressed to obtain cylindrical compacts of 10 mm in diameter and 8 mm high with a density of approximately 50–55% of their theoretical value. As an igniter, a thin (~0.5 mm) layer of Zr + 2B powders was pressed on the top of the reacting pellet in order to ensure a fast ignition, in particular in the reactions with high amounts BN. Experiments were performed in an SHS chamber made of stainless steel, the details of which were reported previously [20, 21]. Before the experiments, three consecutive vacuum-argon cycles were applied; the reaction was conducted under high purity argon at atmospheric pressure. The reaction pellet was ignited from the top by applying 24V to the igniter coil, which was manufactured from Khantal A1 resistance wire. The velocity of propagation of the combustion front was obtained by video recordings of the reaction.

The reacted samples were analyzed by X-ray powder diffraction (XRPD) with a Bruker D8 Advance unit in the step scan mode with 0.02° steps at a rate of 1 second per step and scanning electron microscopy using a Cambridge SEM Stereoscan 200 operated at 30 kV and equipped with a back-scattered electron detector and a Link microprobe.

## Results and discussion

The combustion mode was largely dependent on the amount of BN in the reactants. The variation of the combustion front velocity with Batch-2 content of the reactants is shown in Fig. 2. Increasing the BN amount the reaction front becomes progressively slower. Sample C5 ignited with some difficulty and the reaction front propagated in a non-steady mode (spin combustion). Zr + BN mixture could not be ignited.

Also the overall morphology of the product was largely determined by the amount of BN in the starting mixture. In all cases, the product swelled during the reaction increasing its volume up to 100% for the most exothermic reaction. The sample expansion occurred almost exclusively in the direction of propagation of the reaction front, producing a lamellar morphology as shown in the SEM photographs in Fig. 3(a) and (b), which correspond to samples C1 and C5, respectively. Consequently the products resulted to be particularly fragile. This phenomenon is well known in the SHS literature [22]: extremely exothermic reactions, such as those that lead to the formation of Ti, Zr, and Hf borides, are characterized by a micro-pulsating propagating mode that leads to a crack formation along the propagation wave. The appearance of radial cracks in the combustion products has been addressed to both thermal and mechanical stress caused by pressure increase in pores.

The lamellae thickness was found to be dependent on the starting composition. Comparing Fig. 3(a) and (b) it can be observed that the lamellae thickness increases as the

**Table 1** Expected amounts of $ZrB_2$ and ZrN phases in the produced composite powders and calculated adiabatic temperatures of the reactions

| Sample Idenfitication | Amount of Batch-2 in total reactant mixture (weight %) | Weight % ratios of Constituents of Reactants | | | Expected weight % ratios of the product phases | | Calculated Adiabatic Temperature (°C) [19] |
|---|---|---|---|---|---|---|---|
| | | Zr | B | BN | $ZrB_2$ | ZrN | |
| C1 | 0 | 80.8 | 19.2 | 0.0 | 100 | 0 | 3049.9 |
| C2 | 20 | 81.6 | 15.3 | 3.1 | 87.0 | 13.0 | 3049.9 |
| C3 | 40 | 82.4 | 11.5 | 6.1 | 74.0 | 26.0 | 3049.9 |
| C4 | 60 | 83.1 | 7.7 | 9.2 | 60.9 | 39.1 | 3022.5 |
| C5 | 80 | 83.9 | 3.8 | 12.3 | 47.9 | 52.1 | 2951.9 |
| C6 | 100* | 84.6 | 0.0 | 15.4 | 34.9 | 65.1 | 2876 |

* Could not be ignited

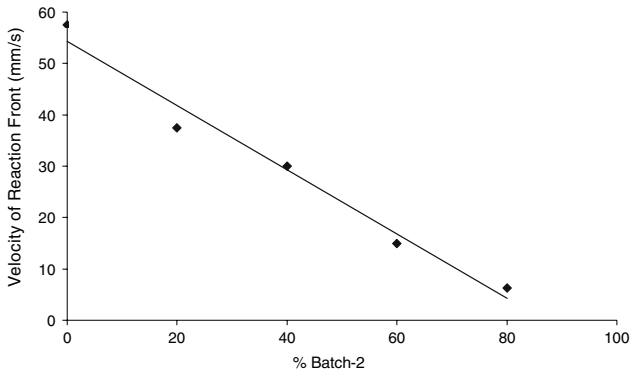


**Fig. 2** Velocity of the SHS reaction wave front as a function of Batch-2 content in the reactant mixture

exothermicity of the reaction decreases. Nonetheless the sample expansion, and the consequent cracking of the product, was considerable even for the least exothermic composition. It must be considered at this regard that BN addition not only causes a decrease in the reaction temperature but also increases the amount of nitrogen released during the reaction (Fig. 3b) increasing the pressure inside the pores that ultimately leads to the crack formation.

Due to the very high temperatures involved in the reactions under investigation a preliminary test was carried out to ascertain possible loss of reactants (in particular nitrogen) in gas form during the passage of the thermal wave. For this purpose the samples were carefully weighted before and after the reaction: no appreciable weight difference was observed. This result was confirmed by XRPD analysis; no unreacted elements were detected in the products (in particular no elemental Zr was found) indicating the completion of the chemical reaction.

The XRD patterns of the reaction products, for all starting compositions, are shown in Fig. 4(a–f). Complete conversion of the reactants into products ($ZrB_2$ and ZrN) was observed in all the reactions regardless the different reaction temperatures. Even in the case of sample C5 that proceeded with the spin propagation mode, full conversion was obtained. According to the reaction stoichiometry, the relative peak heights of the ZrN phase in the product increase as the amount of BN in the initial mixture increases (from sample C1–C5). It was observed that there was no shift in the positions of $ZrB_2$ and ZrN [JCPDS Nos: 34-0423 and 35-0753, respectively] peaks relative to the amounts of the formed $ZrB_2$ and ZrN phases in the products, revealing that there was no solid solution formation between them. This finding is in agreement with the binary phase diagram of $ZrB_2$ and ZrN [23] where it is evident that there is no solubility of $ZrB_2$ and ZrN phases in each other at room temperature.

Small amounts of tetragonal $ZrO_2$ peaks were observed on the XRD patterns of the products. In order to identify its source, variation of the oxide phase with the composition of the reactants was examined. As shown in Table 1, amount of BN increases, amount of B decreases and amount of Zr slightly increases in the reactant mixtures from C1 to C5. However, it was inferred from Fig. 4 that there was no regular trend in the amount of $ZrO_2$ relative to the compositions of the starting mixtures. Considering that the source of oxygen can be either one of the reactants or the argon gas, systematic set of experiments was performed. Since an identical amount of $ZrO_2$ was found in the internal and the external part of the sample and since such amount did not vary by replacing argon atmosphere with nitrogen, the gas source can be excluded. Concerning the internal source (reactants), even though all of the reactants appeared free from oxides at XRPD analysis and drying in a muffle at 150 °C was not beneficial in removing $ZrO_2$ from the product, the presence of dissolved or absorbed oxygen cannot be a priori excluded. In particular Zr can, according to the phase diagram, dissolve a high amount of (30%) oxygen in its structure. Formation of $ZrO_2$ was observed also in other studies [5, 23], where the oxygen was proposed to originate from the partial oxidation of Zr particles before the synthesis reaction due to their

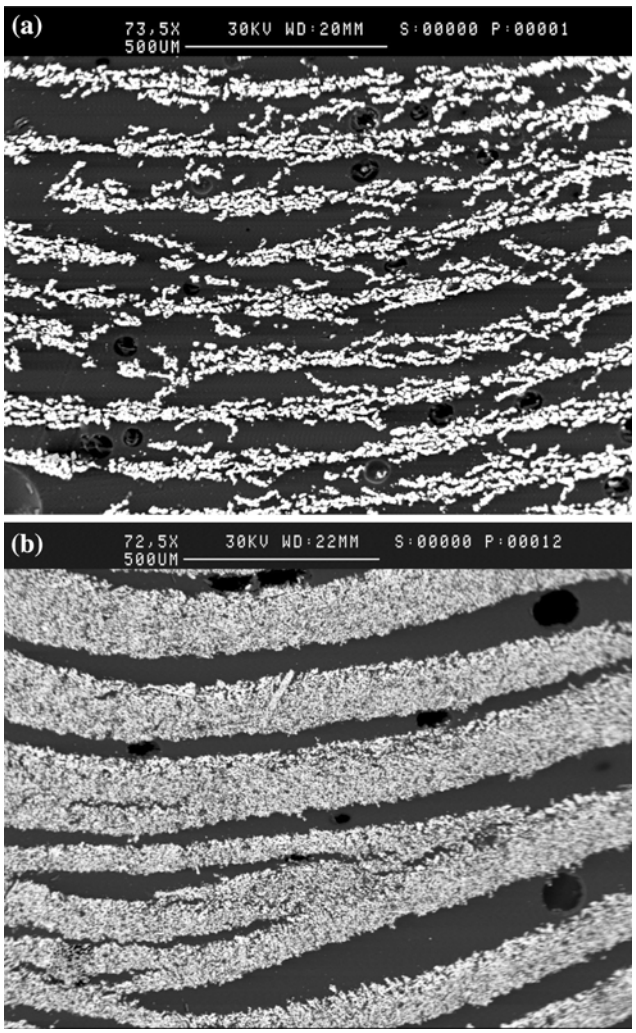


**Fig. 3** Lamellar structure of the product pellets: (**a**) C1 (×73.5), (**b**) C5 (×72.5)

high chemical activity and from the small amount of $B_2O_3$ possibly existing in BN starting powder, respectively.

SEM analyses were conducted to gain information on the particle size and phase distribution in the products and their dependence on reaction temperature. High magnification SEM pictures of the products are shown in Fig. 5(a–e) for all starting mixtures. The $ZrB_2$ grains in the pure Zr + 2B sample (Fig. 5a) are larger than the ones formed with other compositions containing BN; also, a large sintering of the grains is observed for this sample indicating that the actual temperature attained in the pellet was probably close or equal to the melting temperature of $ZrB_2$ (3050 °C). As the amount of BN in the reactants increases, a finer grained second phase (ZrN) which can be seen on the surface of the $ZrB_2$ grains (Fig. 5b–e) increases while $ZrB_2$ sintering appears more and more limited. In the samples containing high amounts of BN in the reactants, the presence of ZrN could be identified also by visual

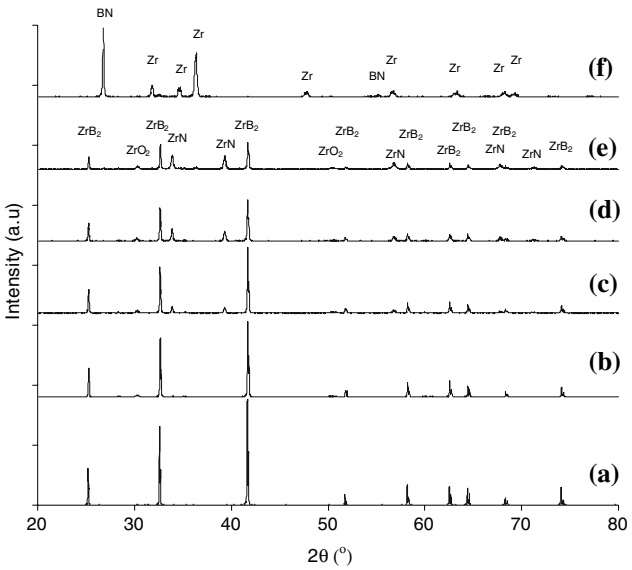


**Fig. 4** XRD patterns of the products of the experiments conducted with samples (**a**) C1, (**b**) C2, (**c**) C3, (**d**) C4, (**e**) C5, (**f**) C6*. *Could not be ignited

observations on the fracture surface of the product pellets, due to the dark yellow color of ZrN grains.

From the examinations on the morphology changes of the formed $ZrB_2$ and ZrN phases taking place in relation to the variation of BN content of the reactant mixture, and also considering the Gibbs free energies of Reactions (1) and (2), a reaction mechanism can be proposed. It may be expected that at the beginning of the reaction, all of the reactants are in solid state, since the maximum temperature that can be attained by the Khantal A1 coil is around 1300–1350 °C, above which the coil would melt. This temperature is well below the melting points of both Zr and B, as presented in Table 2. At this temperature the Gibbs free energy of reaction between solid Zr and B (Reaction (1)) is –69,600 kJ/mol while that of Zr and BN (Reaction (2)) is –40,000 kJ/mol, therefore the occurrence of the first reaction is more favorable. In these calculations data compiled by Turkdogan was used [24]. After the ignition, it can be inferred from the adiabatic temperatures of the reactions given in Table 1 and from the melting points of the reactants presented in Table 2 that the temperature at the reaction front will be above the melting points of Zr and B and also above the dissociation temperature of BN for the samples containing low BN. It should be noted that the actual temperatures are lower than the calculated values, due to the losses of heat mainly by radiation [25]. However, the actual temperatures are still expected to be higher than the melting points of Zr and B for all the compositions. Accordingly, the reaction is expected to proceed first between liquid Zr and B and then between liquid Zr and B, and N formed by the dissociation of BN, in the samples

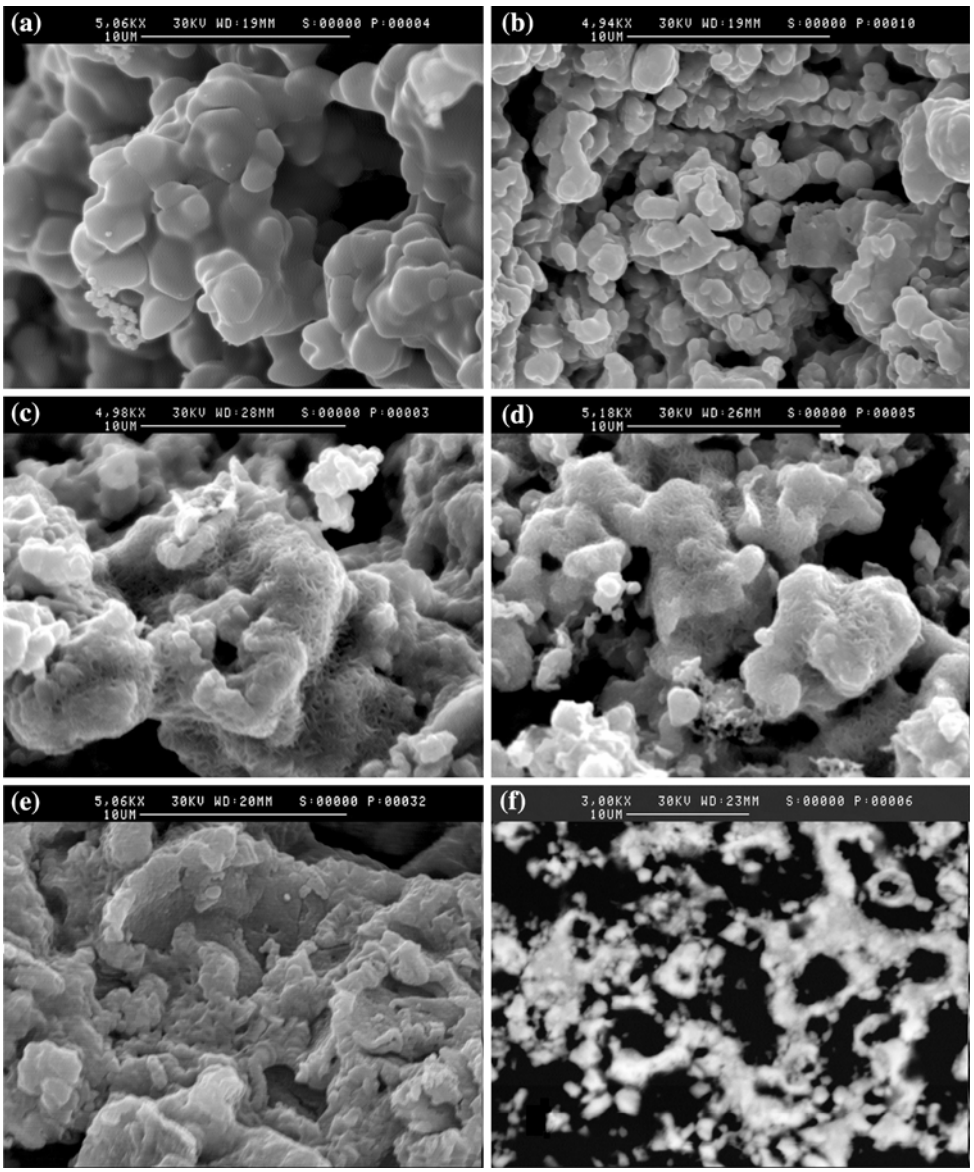


**Fig. 5** SEM micrographs of the products of the experiments conducted with samples (**a**) C1 (×5060), (**b**) C2 (×4940), (**c**) C3 (×4980), (**d**) C4 (×5180), (**e**) C5 (×5060), (**f**) C5 (×3000), mounted in epoxy resin, polished surface, and backscatter mode

**Table 2** Melting and boiling temperatures of the reactants and products [26, $19]

| Matter | Zr | B | BN | $ZrB_2$ | ZrN |
|---|---|---|---|---|---|
| T melting (°C) | 1855 | 2075 | 2966* | 3050$ | 2960 |
| T boiling (°C) | 4409 | 4000 | – | – | – |

* Dissociates into B and N

with low BN content where BN dissociation is possible. For the samples with high BN content, the actual temperature is expected to be lower than the dissociation temperature of BN, thus after the reaction of liquid Zr and B, the reaction is expected to proceed between liquid Zr and solid BN. In both cases, where BN decomposition is possible or not, it is likely that ZrN forms after $ZrB_2$. Due to the fact that $ZrB_2$ has higher melting point than ZrN and that $ZrB_2$ is expected to form before ZrN, the grains of $ZrB_2$ crystallizes first, after which crystallization of ZrN grains occurs among $ZrB_2$ grains. The observations on the SEM micrographs stating that ZrN grains forms over $ZrB_2$ are in favor of this argument.

A backscatter SEM image of polished surface of Sample-C5 is presented in Fig. 5(f). In this micrograph, the black regions are epoxy resin in which the sample was mounted; ZrN phase appears white whereas $ZrB_2$ appears gray, due to its lower Zr content. It can be deduced from this figure that $ZrB_2$ and ZrN phases are homogenously distributed in the composite powder.

The dependence of the crystallite dimensions of $ZrB_2$ and ZrN on BN content in the starting mixture is shown in Fig. 6. The average crystallite dimensions presented in this figure were calculated from XRD patterns according to the

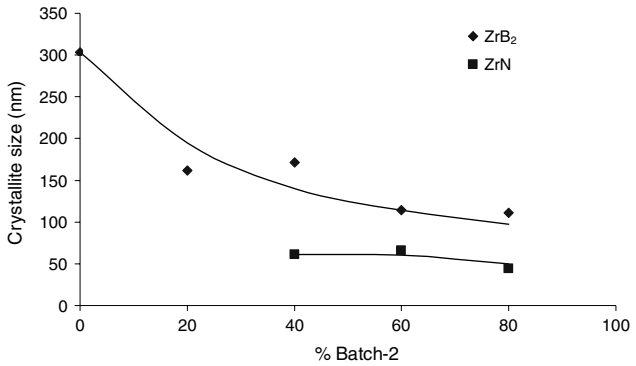


**Fig. 6** Variation of the crystal sizes of $ZrB_2$ and ZrN by Batch-2 content of the initial mixture

Scherrer formula [27]. The broadening of the peaks (full width at half maximum, FWHM) pertaining to the (101) plane for $ZrB_2$ and (111) plane for ZrN were utilized in these calculations. The average crystallite size of $ZrB_2$ decreases on increasing the ZrN phase, in agreement with the adiabatic temperature decrease (Table 1). The variation is particularly evident between the ZrN-free sample and the others with the first showing a grain size 2 times larger. A similar result was observed in the SHS of $TiB_2$–TiN composites [13]; the inhibition of $TiB_2$ grain growth was in that case addressed to the pinning effect of TiN grains. The grain size of ZrN is smaller and also shows a less pronounced variation with composition. This result can be interpreted in the framework of the above proposed reaction mechanism. The ZrN phase formation is the last reactive step and is likely to occur in the post front zone were the temperature is rapidly decreasing.

The difference of the grain sizes of $ZrB_2$ and ZrN phases as appreciated by both SEM and XRPD analysis in the present study is in contrast with what was observed in the study of Zhang et al. [14], where a $ZrB_2$–ZrN composite was prepared by in-situ reactive hot pressing, obtaining a microstructure characterized by similar grain size of the two phases. The above difference can be addressed to the more similar reaction temperature at which the two phases are formed in the hot pressing technique compared to SHS where differences up to several hundred Celsius degrees can be built up between the leading edge of the reaction front (where $ZrB_2$ forms) and even the closest product zone (few microns behind) where the subsequent reactive steps (BN dissociation and ZrN formation) are likely to occur.

## Conclusion

$ZrB_2$–ZrN powder composites with varying proportions were produced by changing the amount of BN in the reactants which consisted of Zr, B and BN. It was seen that adiabatic temperature of the reaction and grain size of the products decreased by increasing the boron nitride in the reactants. The components of produced composite powder mixtures are both hard and high temperature resistant materials. Therefore, similar or improved properties may be expected from the formed composite powders. These powders are candidate materials to be utilized as reinforcements in metal matrix composites or ceramic composites. Homogenously distributed fine grain sized reinforcement phase is a general requirement in these composites. In this respect, to be used in composites, the most suitable powder mixture produced in the present study can be the one formed from the mixture containing 80% Batch2, sample C5. However, properties of the composites are also expected to alter due to the composition of the reinforcement powder. Therefore, the dependence of the properties of composites on the composition as well as on the grain size of the produced composite powders is of interest. Studies on sintering of the produced composite powders are in progress.

**Acknowledgements** One of the authors, H. E. Camurlu wishes to thank to the staff of the Physical Chemistry Department of University of Pavia, Italy for giving him the opportunity of studying in their department as a visiting scientist and Akdeniz University Research Funds for their financial support.

## References

1. Bansal NP (2005) in Handbook of ceramic composites. Kluwer Academic Publishers, Boston, p 211
2. Low IM (1991) Key Eng Mater 53–55:592
3. Khanra AK, Pathak LC, Mishra SK, Godkhindi MM (2003) J Mater Sci Lett 22:1189
4. Pierson HO (1996) in Handbook of refractory carbides and nitrides. Noyes Publications, New Jersey, p 197
5. Radev DD, Marinov M (1996) J Alloy Compd 244:48
6. Radev DD, Klissurski D (2001) J Mater Synth Process 9:131
7. Feng HJ, Moore JJ, Wirth DG (1992) Int J Self-Propag High-Temp Synt 1:228
8. Patil KC, Aruna ST, Mimani T (2002) Curr Opin Solid St M 6:507
9. Tsuchida T, Kawaguchi M, Kodaira K (1997) Solid State Ionics 101–103:149
10. Tsuchida T, Yamamoto S (2004) J Eur Ceram Soc 24:45
11. Breval E, Johnson WB (1992) J Am Ceram Soc 75:2139
12. Monteverde F, Bellosi A, Guicciardi S (2002) J Eur Ceram Soc 22:279
13. Tomoshige R, Murayama A, Matsushita T (1997) J Am Ceram Soc 80:761
14. Zhang GJ, Ando M, Yang JF, Ohji T, Kanzaki S (2004) J Eur Ceram Soc 24:171
15. Zhao H, Wang J, Zhu Z, Wang J, Pan W (2006) J Mater Sci 41:1769
16. Munir ZA (1988) Am Ceram Soc Bull 67:342
17. Mishra SK, Das S, Pathak LC (2004) Mater Sci Eng A364:249
18. Khanra AK, Godkhindi MM, Pathak LC (2005) J Am Ceram Soc 88:1619

19. HSC Chemistry for Windows-Chemical Reaction and Equilibrium Software, Outokumpu Research Oy, Pori, Finland, 1999
20. Maglia F, Milanese C, Anselmi-Tamburini U, Munir ZA (2003) J Mater Res 18:1842
21. Anselmi-Tamburini U, Arimondi M, Maglia F, Munir ZA (1998) J Am Ceram Soc 81:1765
22. Makino A (2001) Prog Energ Combust 27:1
23. Ordanyan SS, Chupow VD (1894) Inorg Mater 20:1719
24. Turkdogan ET (1980) in Physical chemistry of high temperature technology. Academic Press, London, pp 5–24
25. Bertolino N, Monagheddu M, Tacca A, Guiliani P, Zanotti C, Maglia F, Anselmi-Tamburini U (2003) J Mater Res 18:448
26. Handbook of chemistry and physics, 67th ed. CRC Press, Bora Raton, FL
27. Cullity BD, Stock SR (2001) in Elements of X-ray diffraction. Prentice Hall, New Jersey, p 169